Available online at www.sciencedirect.com
ScienceDirect
Journal of Molecular Catalysis A: Chemical 259 (2006) 328–335
JOURNAL OF MOLECULAR CATALYSIS A: CHEMICAL
www.elsevier.com/locate/molcata

Preparation and evaluation of porous nickel-alumina spheres as catalyst in the production of hydrogen from decomposition of methane

Rusiene M. de Almeida [a], Humberto V. Fajardo [a,*], Daniela Z. Mezalira [a], Giselle B. Nuernberg [a], Lúcia K. Noda [a], Luiz F.D. Probst [a], Neftalí L.V. Carreño [b]

[a] *Universidade Federal de Santa Catarina, Centro de Ciências Físicas e Matemáticas, Departamento de Química, Pós-Graduação em Química, Campus Universitário, CP 476, CEP 88040-900, Trindade, Florianópolis, SC, Brazil*
[b] *Departamento de Química Analítica e Inorgânica, Universidade Federal de Pelotas, 96010-900, Pelotas, RS, Brazil*

Received 23 May 2006; received in revised form 13 July 2006; accepted 14 July 2006
Available online 30 August 2006

Abstract

This paper presents the synthesis of Al_2O_3 and Ni-doped Al_2O_3 spherical catalysts, developed by our group, with porous structures and high surface areas. The catalytic activity of the materials obtained was evaluated in the catalytic decomposition of methane, which is an attractive method for CO/CO_2-free production of hydrogen, particularly for fuel cell applications. The catalysts were shown to be active and stable in relation to the catalytic decomposition of methane reaction. After the catalytic tests, characterization of the deposited carbon was carried out by transmission electron microscopy, scanning electron microscopy and Raman spectroscopy. The analyses indicated the presence of single-walled nanotubes (SWNTs) and multiwalled nanotubes (MWNTs). It was observed that the catalytic behaviour and the form of carbon produced depend on the characteristics of the sites present on the catalyst surface and on the operational conditions employed.

Keywords: Alumina; Methane; Hydrogen production; Carbon nanotubes

1. Introduction

Hydrogen is considered to be the energy carrier of the future and its production is a subject of current interest for fuel cell applications where it is the preferred fuel. For stationary applications, the most convenient source of hydrogen for fuel cells at the present time is natural gas, because of its availability and low cost [1–5]. Among the possible natural gas processing technologies, the direct catalyzed decomposition of methane has recently been receiving attention as an alternative route to the production of CO/CO_2-free hydrogen. Unlike other conventional hydrogen production methods, such as methane steam reforming and methane partial oxidation, which produce a mixture of hydrogen and carbon oxides, catalytic cracking produces hydrogen and solid carbon, thereby eliminating the necessity for the separation of hydrogen from the other gaseous products. This significantly simplifies the process, reduces overall CO_2 emissions and makes it particularly attractive for fuel cell applications [3–14]. In addition, the decomposition of methane also results in the generation of a very important byproduct, nanocarbon materials (carbon nanotubes and nanofibers), that have been paid considerable attention due to their excellent properties and potential utilizations [15–18]. The potential uses of the nanocarbons depend on their textures and structures; therefore, another goal of the process is to monitor the features of the carbon formed.

In previous studies, several catalysts have been proposed to be further considered for practical applications in direct decomposition of methane. Shah et al. [11] presented the results for the catalytic decomposition of undiluted methane into hydrogen and carbon using nanoscale Fe-M (M = Pd, Mo or Ni) catalysts supported on alumina. These binary catalysts reduced the methane decomposition temperature by 400–500 °C relative to thermal methane cracking and they were more active than a monometallic $5\%Fe/Al_2O_3$ catalyst. In addition, the form of carbon produced is different at different decomposition tempera-

* Corresponding author. Tel.: +55 48 3331 9966; fax: +55 48 3331 9711.
E-mail address: hfajardo@qmc.ufsc.br (H.V. Fajardo).

1381-1169/$ – see front matter © 2006 Elsevier B.V. All rights reserved.
doi:10.1016/j.molcata.2006.07.044

tures and in the temperature range where the catalysts were most active; multiwalled carbon nanotubes were the dominant form of carbon produced. Muradov [12] has studied direct cracking of methane over different samples of elemental carbon, including a variety of activated carbons, carbon blacks, nanostructured carbons, graphites, glassy carbon and synthetic diamond powders. It was demonstrated that carbon materials are capable of producing hydrogen-rich gases at moderate temperatures. Although activated carbons are initially more active than carbon blacks, the latter result in a more sustainable process of methane decomposition and the catalytic activity of carbons is mostly determined by their origin and surface properties.

Most of the metal supported catalysts for methane decomposition reported until now were prepared by impregnation of commercial supports with a solution of the salt of the active component or by co-precipitation of salts of the active component and a textural promoter. In this context, this paper presents the synthesis of spherical Al_2O_3 and Ni-doped Al_2O_3 catalysts with porous structures, containing mainly mesopores, with a high surface area. The synthesis method for the spherical catalysts developed by our group consists of obtaining a hybrid spherical compound of aluminum hydroxide and the organic polymer chitosan. Through the polymer elimination by thermal treatment, a porous Al_2O_3 sphere is obtained [19]. With the aim of highlighting the enhancement of catalytic properties, the catalysts obtained were tested in the decomposition of methane reaction for hydrogen production. After the catalytic tests, characterization of the deposited carbon was carried out and the results are reported here.

2. Experimental

2.1. Catalyst preparation

For the Al_2O_3 spheres preparation, 1.50 g of chitosan $(C_6H_{11}O_4N)_n$ (Aldrich) was dissolved in 50 mL of acetic acid solution (5%, v/v) and 4.60 g of $Al(NO_3)_3{\cdot}9H_2O$ (Riedel-de-Haën) were dissolved in 20 mL of distilled water. The Al aqueous solution was then added to the polymer solution with stirring. The chitosan monomer to Al molar ratio was 1.5–2. The Al–chitosan solution was added into a NH_4OH solution (50%, v/v) under vigorous stirring, in the form of drops with a syringe pump. The gel spheres formed were removed from the NH_4OH solution and dried at ambient temperature for 72 h. The nickel addition (5 wt.%) was carried out by impregnation of an aqueous solution of $Ni(NO_3)_2{\cdot}6H_2O$ (Fluka, 98%) on the Al_2O_3 spheres with stirring for 6 h. The samples with nickel were dried at ambient temperature for 24 h. The Al_2O_3 (Al_2O_3#350, Al_2O_3#550 and Al_2O_3#700) and Ni/Al_2O_3 (Ni/Al_2O_3#550 and Ni/Al_2O_3#700) samples were obtained by calcining the dried samples at 350, 550 and 700 °C in air flow for 1 h with a heating rate of 5 °C/min.

2.2. Sample characterization

Samples were characterized by N_2 adsorption/desorption isotherms obtained at the temperature of liquid nitrogen in an automated physisorption instrument (Autosorb-1C, Quantachrome Instruments). Prior to the measurement, the samples were outgassed in vacuum at 200 °C for 2 h. Specific surface areas were calculated according to the Brunauer–Emmett–Teller (BET) method, and the pore size distributions were obtained according to the Barret–Joyner–Halenda (BJH) method from the adsorption data.

For the determination of the Ni content an atomic spectrometer (Varian Model SpectrAA 50), equipped with an air–acetylene flame atomizer and a Hitachi hollow cathode lamp (HLA-4S) was used. The instrument parameters were: wavelength 232 nm, slit width 1.0 nm, lamp current 4 mA, aspiration rate 5 mL/min and fuel acetylene with support air. The standard solutions for the Ni ion were prepared through appropriate dilution of a stock solution (Merck) containing 1000 ppm.

Temperature programmed reduction (TPR) analysis was performed in a quartz reactor under 5 vol.% H_2/N_2 flow (30 mL/min) from 30 to 920 °C at a heating rate of 5 °C/min. A thermal conductivity detector (TCD) was used to monitor the H_2 consumption. A PM5A column trapped water formed during the process.

The crystalline phases (of freshly prepared catalysts and their reduced forms) were characterized by X-ray diffraction (XRD) in a Siemens D-5000, with graphite monochromated Cu Kα irradiation.

The sample morphology was observed with scanning electron micrographs, obtained with a Philips XL30 scanning microscope operating at an accelerating voltage of 20 kV.

2.3. Catalyst testing

The decomposition reaction of CH_4 (Scheme 1) was carried out in a quartz-tube fixed bed flow reactor (12 mm inner diameter) heated by an electric furnace. The Ni/Al_2O_3 spheres (100 mg), heat-treated at 550 and 700 °C, were pre-treated in situ in a H_2 stream at 700 °C (with a heating rate of 10 °C/min) for 1 h. The experiments were conducted under atmospheric pressure at 600, 700 and 800 °C. The reaction gas was composed of N_2 and CH_4 in a 6:1 molar ratio. The total flow rate of the reaction gas was 70 mL/min. The reactant and the product gases were

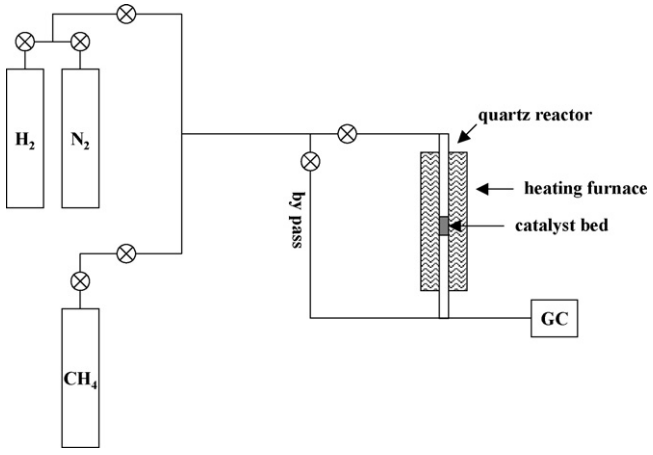

Scheme 1. Schematic diagram of the reactor system.

analyzed with a Shimadzu GC-8A gas chromatograph, equipped with a TCD, Porapak-Q and a 5A molecular sieve column with Ar as the carrier gas. The N_2 in the reaction gas was used as a diluent and as an internal analysis standard. Catalytic activity was evaluated in terms of methane conversion. We defined methane conversion as:

$$C(CH_4) = \frac{Q_{conv}}{Q_{CH_4}} \times 100\% \quad (1)$$

where Q_{conv} represents the quantity (moles) of converted methane; Q_{CH_4} represents the total quantity (moles) of methane fed into the reactor.

2.4. Sample characterization after catalyst testing

The specific surface areas of the samples used were calculated according to the Brunauer–Emmett–Teller (BET) method and the pore volumes were obtained according to the Barret–Joyner–Halenda (BJH) method from the adsorption data.

The structure, texture and morphology of the deposited carbon were characterized by means of Raman spectroscopy (Renishaw Raman System 3000) at room temperature. Spectra were recorded using the 632.2 nm excitation line of a Spectra Physics He–Ne laser. Transmission electron microscopy (TEM) images were obtained in a Philips CM 200 microscope operating at 200 kV. Scanning electron micrographs (SEM) were obtained with a Philips SEM-505 scanning microscope operating at an accelerating voltage of 20 kV.

3. Results and discussion

3.1. Catalysts characterization

The spheres were heat-treated at 350, 550 and 700 °C under airflow for 1 h. After calcinations at 350 °C, the Al_2O_3 sample had a black colour, indicating the presence of residual carbon. On the other hand, the samples heat-treated at 550 and 700 °C had a white colour and for the Ni/Al_2O_3 samples a light green colour was observed after the heat-treatment, which indicates the elimination of carbon at high temperatures (550 and 700 °C). The N_2 adsorption/desorption isotherms of the Al_2O_3 samples heat-treated at 550 and 700 °C show type-IV (IUPAC) curves, pointing to the mesoporous material. By contrast, the Al_2O_3 sample heat-treated at 350 °C shows a microporous isotherm (Fig. 1a). The N_2 adsorption/desorption isotherms of the Ni/Al_2O_3 samples (Fig. 1b) indicate a change in the patterns due to nickel addition. The profile suggests a change from a mesoporous to a macroporous material and lowering of the surface areas (Table 1). The pore size distributions of the samples (Fig. 2) confirm the presence of micropores for the sample heat treated at 350 °C, but with an increase in the calcination temperature mesopore formation is significantly favored. This behaviour is attributed to carbon elimination at the higher treatment temperatures. With a heat treatment at 350 °C, the amount of residual material is still high. However, as summarized in Table 1, the higher surface area and the lower total pore volume of the sample heat treated at 350 °C may be due to the small pore size. The residual carbon elimination by heating at 550 and 700 °C resulted in a surface area decrease and thus, the residual carbon is thought to contribute significantly to a higher surface area. On the other hand, the carbon elimination promoted a great increase

Table 1
Chemical analysis and surface properties measured by N_2 physisorption

Samples	T_c# (°C)	Ni (wt.%)	S ($m^2\ g^{-1}$)	V_p ($cm^3\ g^{-1}$)
Al_2O_3	350	–	464	0.354
Al_2O_3	550	–	343	0.651
Al_2O_3	700	–	313	0.581
Ni/Al_2O_3	550	3.8	270	0.560
Ni/Al_2O_3	700	3.8	210	0.430

T_c#, temperature of calcinations; S, specific surface area; V_p, pore volume.

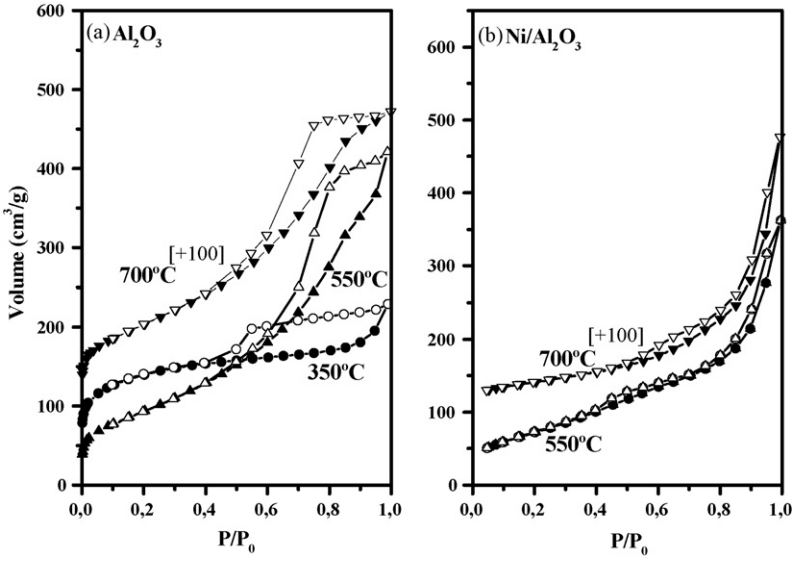

Fig. 1. Nitrogen adsorption/desorption isotherms of samples heat-treated at different temperatures: (a) Al_2O_3 and (b) Ni/Al_2O_3. Closed symbols for adsorption, open symbols for desorption branch. Isotherms of samples heat-treated at 700 °C are vertically shifted 100 cm^3/g for clarity.

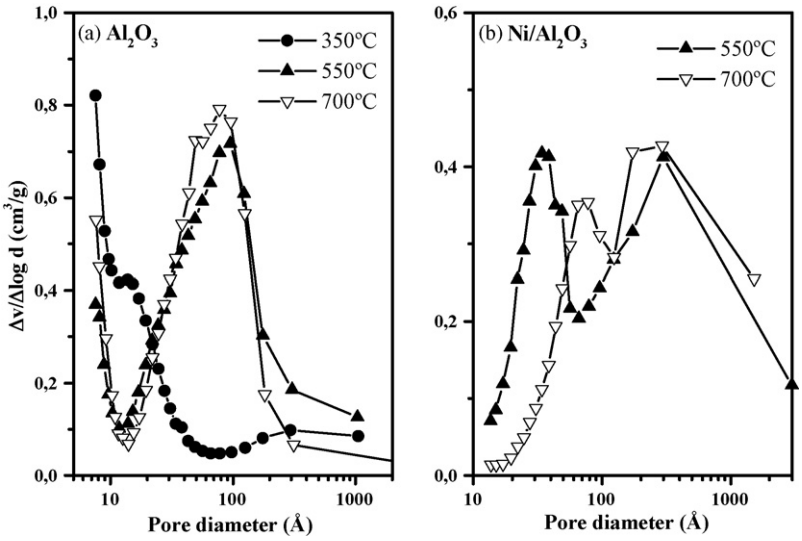

Fig. 2. Pore diameter distribution of the samples heat-treated at different temperatures: (a) Al_2O_3 and (b) Ni/Al_2O_3, calculated using the BJH model from the adsorption branch.

in the total pore volume, which suggests that the residual carbon present within the pores of the crystalline matrix is an amorphous carbon with high surface area. Burning off the residual carbon generated pores, which leads to mesopore formation and an increase in the total pore volume. The Ni doped Al_2O_3 sphere samples also presented a high surface area and pore volume. However, as shown in Table 1, these values were lower than those for the Al_2O_3 samples. The comparison of pore size distributions of Al_2O_3 and Ni/Al_2O_3 (Fig. 2a and b) shows clearly a difference in their pore sizes. The presence of nickel promoted the obtention of a sphere with meso- and macropores. Such a change in the pore size distribution cannot be attributed totally to the pore closing due to the NiO. As indicated by the hysteresis of the isotherms in Fig. 1b, the pore shapes of the Ni/Al_2O_3 samples appear to be slitlike. The presence of nickel promotes faster carbon elimination and such behaviour certainly affects the type of pores formed during the heat-treatment [19,20].

With the aim of identifying the phases present in the catalytic samples, X-ray diffraction and TPR analysis were carried out. Despite the $NiAl_2O_4$ and γ-Al_2O_3 peaks being overlaid, in the XRD results of the freshly prepared catalysts presented in Fig. 3a the profiles show the $NiAl_2O_4$ formation, which is clearer for the sample heat treated at 700 °C. The XRD results also indicate the presence of the NiO phase. This suggests the possibility of obtaining catalytic sites with different properties after the activation. The shifts in the peaks at $2\theta = 45°$ and 66° are greater for the Ni/Al_2O_3 sample heat treated at 700 °C due to the presence of $NiAl_2O_4$, which means that the $NiAl_2O_4$ phase formation is greater for this sample. Fig. 3b shows the results of the XRD analysis of the reduced form of the catalysts. For the Ni/Al_2O_3#550 catalyst there were more intense diffraction peaks related to the crystalline planes (1 1 1), (2 0 0) and (2 2 2) of the Ni, in comparison to the Ni/Al_2O_3#700 catalyst, indicating that the Ni/Al_2O_3#550 catalyst can be reduced more easily. In addition, a decrease in the intensity of the peaks corresponding to the crystalline planes of the Ni was observed for the Ni/Al_2O_3#700 catalyst due to the presence of a strong metal–support interaction resulting from the high temperature of the heat treatment applied to the material.

The determination of reducible species at the surface of the catalyst and the temperature at which these species are reduced,

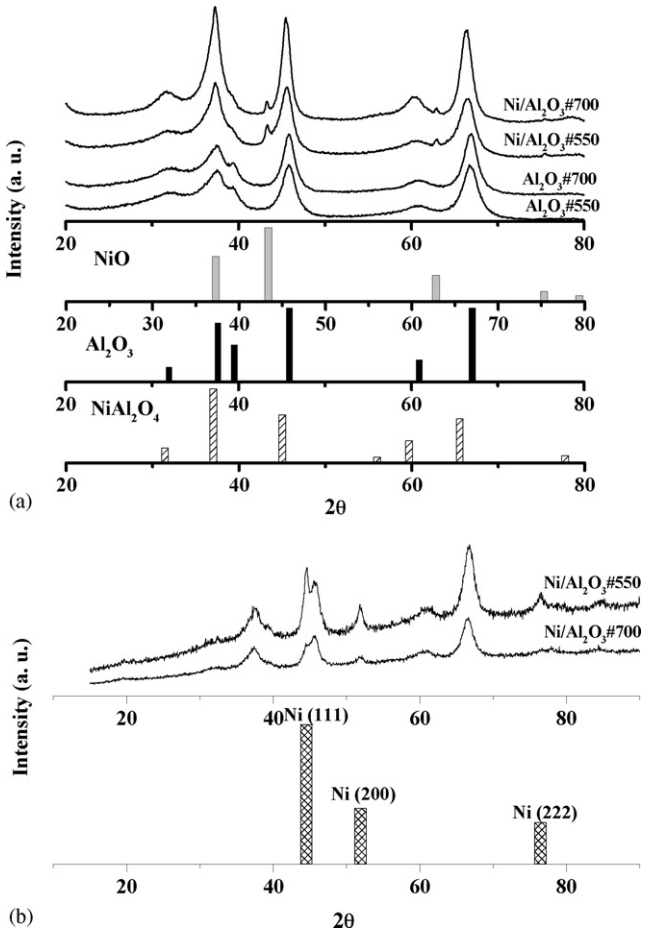

Fig. 3. X-ray diffraction patterns for the (a) samples after the pyrolysis step and (b) catalysts in the reduced form.

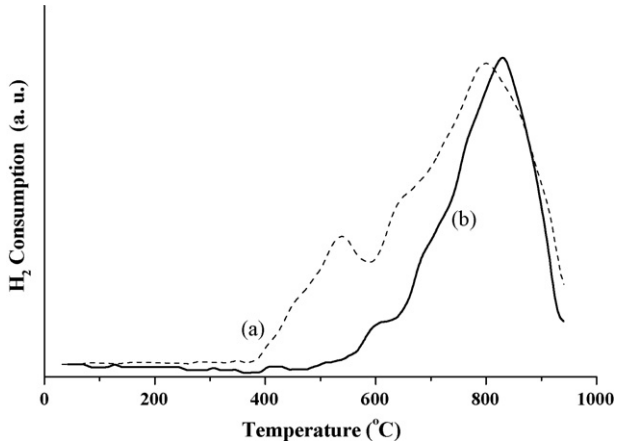

Fig. 4. Temperature programmed reduction profiles of Ni/Al_2O_3 samples: (a) Ni/Al_2O_3 heat-treated at 550 °C and (b) Ni/Al_2O_3 heat-treated at 700 °C.

gives important information on catalysis. The H_2 consumption peak near 530 °C and the shoulder near 630 °C in the TPR profile (Fig. 4) for the Ni/Al_2O_3 sample heat treated at 550 °C are due to the presence of NiO. For the Ni/Al_2O_3 sample heat treated at 700 °C, H_2 consumption was observed at these temperatures but it was significantly lower, indicating that there is less NiO in this sample than in the sample heat treated at 550 °C. The Ni/Al_2O_3 sample heat treated at 700 °C gave a wide range of H_2 consumption, beginning at 450 °C until the final temperature of the process. However, the maximum H_2 consumption peak was observed at 830 °C, which is characteristic of the $NiAl_2O_4$ phase, indicating a greater metal–support interaction, promoted by the calcination temperature applied to the material. This observation is in agreement with the XRD profile, which indicates the presence of the NiO and $NiAl_2O_4$ phases.

Scanning electron microscopy (SEM) was carried out in order to observe the typical morphologies of the samples obtained. The SEM images presented in Fig. 5a and b show the Al_2O_3 spheres heat-treated at 550 °C before the catalyst tests. The SEM image presented in Fig. 5a shows a pore diameter size quite different to that determined by the N_2 adsorption isotherm, but it can illustrate the morphology, which is due to the utilization of organic precursor in the catalyst preparation. During the pyrolysis step the elimination of volatile materials occurs, which produces cavities as a result of their removal. At the same time, a solid rearrangement takes place, forming the crystalline matrix.

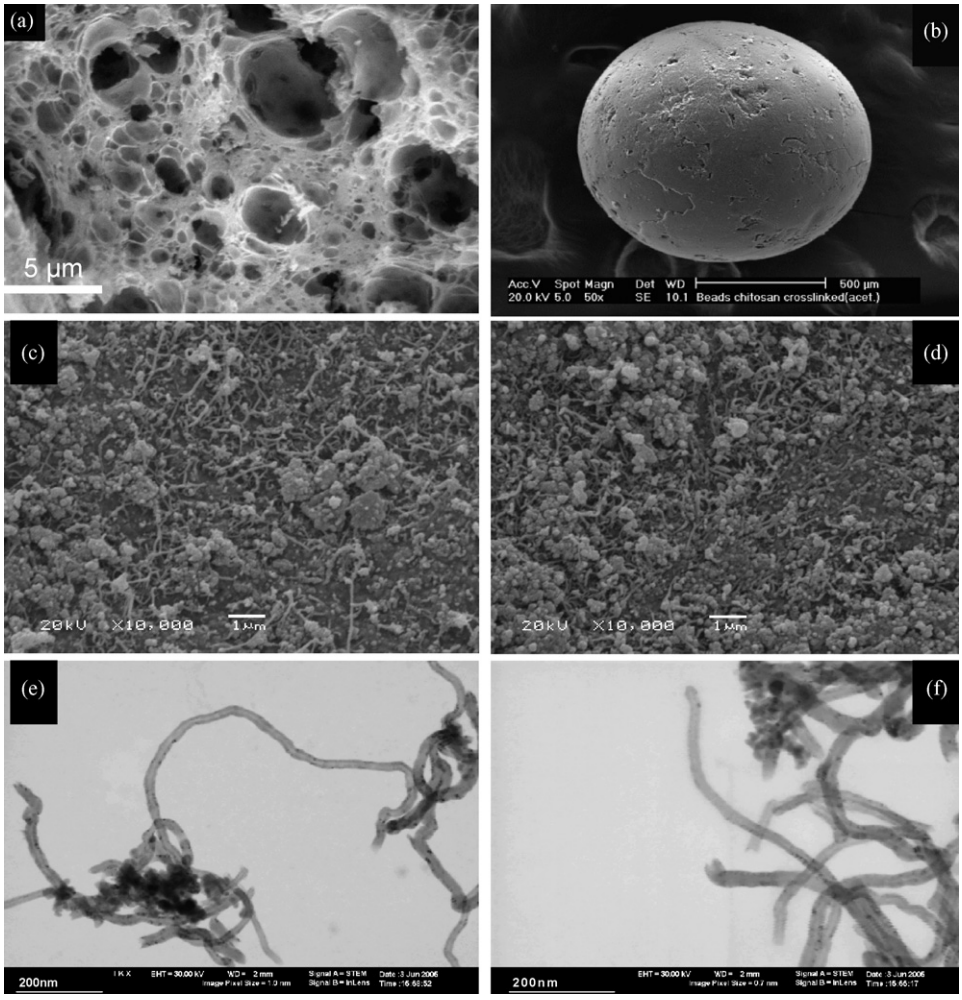

Fig. 5. SEM and TEM images of the catalyst surfaces before and after the reaction: (a and b) spheres heat-treated at 550 °C before reaction, (c and d) Ni/Al_2O_3 samples heat treated at 550 °C after catalytic test at 700 °C and (e and f) TEM images of Ni/Al_2O_3 samples heat treated at 550 °C after catalytic test at 700 °C.

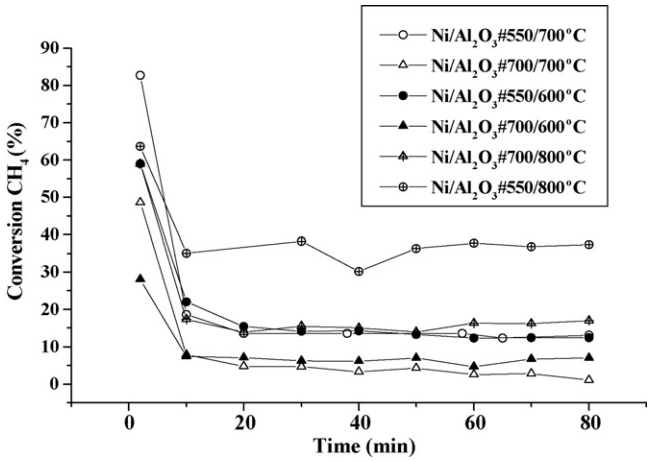

Fig. 6. Methane decomposition over Ni/Al_2O_3 spheres. Performances for the catalysts on CH_4 conversion with time-on-stream at different temperatures.

3.2. Catalyst testing

In order to investigate the catalytic activity of the Ni/Al_2O_3 spheres (Ni/Al_2O_3 heat treated at 550 °C and Ni/Al_2O_3 heat treated at 700 °C) the decomposition reaction of methane was carried out. All tests were conducted under identical experimental conditions and the reactions were run for 90 min. No methane decomposition products other than hydrogen were detected in the effluent gas during the experiments, thus carbon and hydrogen can be regarded as the only products of methane decomposition, that is, only the following reaction occurs during the process:

$$CH_4 \rightarrow C + 2H_2 \quad \Delta H^\circ = 75.6\,\text{kJ/mol} \tag{2}$$

Fig. 6 shows the general performance of Ni/Al_2O_3 catalysts on methane decomposition at different temperatures (600, 700 and 800 °C). Over both Ni/Al_2O_3 catalysts, the initial conversion values of methane decomposition increase as the temperature increases. The Ni/Al_2O_3 catalyst heat treated at 550 °C, at a reaction temperature of 700 °C, showed the highest initial activity on methane decomposition while that for the Ni/Al_2O_3 catalyst heat treated at 700 °C with a reaction temperature of 600 °C was the lowest.

High initial decomposition values presented by both Ni/Al_2O_3 catalysts were followed by a rapid drop in catalytic activity, reaching a quasi-steady-state rate (over 10–20 min) which remained stable for several minutes. This behaviour may be related to the carbon deposition that promotes a blocking of the active surface [10,17]. During the catalytic decomposition reaction, methane molecules are initially adsorbed and decomposed on the metal surface of the catalyst particle, resulting in the formation of chemisorbed carbon species and the release of gaseous hydrogen; the carbon species proceed to dissolve and diffuse through the bulk of the metal particle. Deactivation occurs when the rate of carbon diffusion through the metal catalyst particle is slower than that of the formation of carbon at the surface of the Ni^0 sites. Under these circumstances, carbon builds up at the catalyst surface and eventually encapsulates the metal particle that causes activity loss [17,18]. However, it is interesting to note that the activity is different for different catalysts, the activity being dependent on the catalyst and reaction temperature. For example, the CH_4 conversion presented by the Ni/Al_2O_3 catalyst heat treated at 550 °C, at a reaction temperature of 800 °C, remains near 20% higher than that of the Ni/Al_2O_3 catalyst heat treated at 700 °C, at the same reaction temperature, after 20 min of time-on-stream. This behaviour may be related to the formation of catalytic sites with different characteristics on the surface of the samples (confirmed by TPR and XRD analyses) promoted by the different calcination temperatures to which the material was exposed. The commonly accepted mechanism for methane decomposition over nickel catalysts includes stages of activation and decomposition of methane on the metal surface. The reaction starts with the dissociative adsorption of the methane molecule on the surface of the active sites [6]:

$$(CH_4)_g \rightarrow (CH_3)_a + (H)_a \tag{3}$$

This is followed by a series of stepwise surface dissociation reactions leading to elemental carbon and hydrogen:

$$(CH_{3-x})_a \rightarrow (CH_{2-x})_a + (H)_a \tag{4}$$

$$(C)_a \rightarrow \tfrac{1}{n}(C_n)_c \quad \text{(carbon crystalline growth)} \tag{5}$$

$$2(H)_a \rightarrow (H_2)_g, \tag{6}$$

where, $0 < x < 2$, subscripts (a), (c) and (g) denote adsorbed, crystalline and gaseous species, respectively.

From the results of Fig. 3b, one can see that the Ni/Al_2O_3 catalyst heat treated at 550 °C shows the largest relative intensity of Ni (1 1 1), (2 0 0) and (2 2 2) planes, which may be the reason why it shows the highest capacity for methane decomposition. In this sense, the active phase is more accessible (or evident) in the Ni/Al_2O_3 sample heat treated at 550 °C; as a consequence the catalyst is able to maintain its high activity. In the presence of Ni, the catalyst becomes more active and the active metal site is responsible for the breaking of the C–H bonds in the CH_4 cleavage to produce H_2. On the other hand, the $NiAl_2O_4$ phase formation (indicating a greater metal–support interaction) presented by the Ni/Al_2O_3 sample heat treated at 700 °C decreases the concentration of the active component in the catalyst and this is presumed to difficult methane adsorption on the metal surface of the catalyst particle. This phenomenon may be responsible for the low CH_4 conversion observed over this catalyst.

3.3. Sample characterization after catalyst tests

The changes in the surface properties, including pore properties and surface images were measured for the fresh and used Ni/Al_2O_3 catalysts. Some of their surface properties are summarized in Table 2 and the SEM and TEM images are shown in Fig. 5c–f. For both catalysts, the BET surface areas are all significantly reduced after reaction in the methane stream. For example, the BET surface area of the Ni/Al_2O_3 catalyst heat treated at 550 °C, after a reaction at temperature of 800 °C, decreases from 270 to 156 m^2/g. This may be related to it showing the highest activity during the methane decomposition that

Table 2
Surface properties changes of Ni/Al_2O_3 catalysts after methane decomposition during 90 min at different temperatures

	Ni/Al_2O_3#550			Ni/Al_2O_3#700		
	600[a]	700[a]	800[a]	600[a]	700[a]	800[a]
S ($m^2\ g^{-1}$)	221	202	156	192	161	130
V_p ($cm^3\ g^{-1}$)	0.297	0.307	0.245	0.290	0.282	0.224

[a] Reaction temperature (°C).

leads to the greatest decrease in surface area. The pore volume also decreases for both catalysts after the decomposition reaction. These phenomena result from the carbon deposition especially in the pores of Ni/Al_2O_3 catalysts, which contribute greatly to the surface area and pore volume characteristics of Ni/Al_2O_3 catalysts.

These observations are confirmed by the SEM images that show the changes in the surface of the Ni/Al_2O_3 samples after catalyst tests (shown in Fig. 5c and d), where carbon deposition is clearly seen on the sample surface. Also, the carbon produced using the Ni/Al_2O_3 catalysts was of different types distinguished by the naked eye. A part of the carbon deposition is in the form of carbon filaments and another part is in an irregular agglomerate form. The TEM images of the Ni/Al_2O_3 samples heat treated at 550 °C after catalytic testing at 700 °C (Fig. 5e and f) indicate abundant carbon nanotubes growing out of the Ni particles. The carbon nanotubes grow in a random direction and tend to take the form of arcs.

The Raman spectra of the catalysts after the catalytic tests are shown in Fig. 7. The spectra present bands originated from carbon structures. A band at 1587 cm^{-1} is due to the tangential C–C stretching (G mode); another at 1321 cm^{-1} is the D mode, attributed to disordered carbon structures, present in carbon nanotubes or other carbon forms, with its overtone at 2609 cm^{-1}. The Raman spectra of the Ni/Al_2O_3 catalyst heat treated at 550 °C, after the catalytic tests at 700 and 800 °C, and the Ni/Al_2O_3 catalyst heat treated at 700 °C, after the catalytic tests at 800 °C, show the presence of a low frequency band near 188 cm^{-1}, attributed to the radial breathing mode (RBM) of the carbon nanotubes, characteristic of single-walled nanotubes (SWNTs) [21], however, with a low degree of purity, as can be inferred from the low relative intensity of the G and D bands (IG/ID), of approximately 2. It is known that the higher intensity IG/ID ratio, the more perfect and purer are the SWNTs [21,22]. For the Ni/Al_2O_3 catalyst heat treated at 700 °C, after the catalytic tests at 600 and 700 °C, the spectra indicate only the presence of multiwalled nanotubes (MWNTs) or other carbon forms, because of the negligible intensity of the RBM. The absence of SWNTs for this catalyst may be related to the presence of catalytic sites with different properties on the surface of this sample mainly due to the more intense $NiAl_2O_4$ phase presence. In this case, the active phase (Ni^0) is expected to be less accessible (or available) and the growth of the carbon nanotubes would be inhibited. These results suggest that the mechanism of carbon deposition on the Ni/Al_2O_3#550 catalyst is different from that on the Ni/Al_2O_3#700 catalyst. It is generally agreed that diffusion of carbon through the catalyst particle is the rate-determining step in the growth of nanocarbons [17]. Therefore, according to the above results, the diffusion of carbon is affected not only by the reaction temperature but also by the fraction of Ni^0 sites on the surface of the catalysts. The growth condition for SWNTs is a bit more rigorous than that for MWNTs, which need a higher temperature and are more dependent on the characteristics of the catalytic sites.

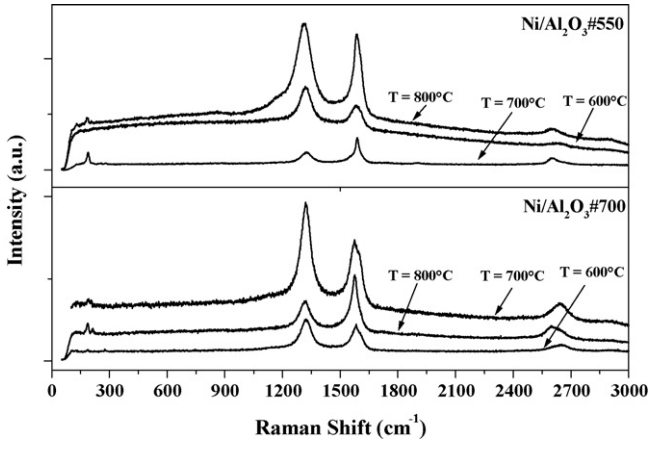

Fig. 7. Raman spectra of the Ni/Al_2O_3 samples after the catalytic decomposition of methane.

4. Conclusions

It was observed that the methodology used in the preparation of Al_2O_3 and Ni/Al_2O_3 spheres led to the obtention of materials with important properties for applications in catalytic processes, such as decomposition of methane. The results clarify that the Ni/Al_2O_3 catalysts were active and stable in relation to the decomposition of methane reaction for the production of hydrogen. This process produces CO/CO_2-free hydrogen in a single step, which is a very attractive feature for fuel cell applications and tests with the objective of evaluating the catalytic stability of the Ni/Al_2O_3 catalysts are being carried out. Carbon, as a valuable byproduct of the process, could potentially significantly reduce the net cost of hydrogen production. After the catalytic tests, we carried out the characterization of the deposited carbon by TEM, SEM and Raman spectroscopy. The analyses indicated the presence of SWNTs and MWNTs. It was observed that the production of SWNTs and MWNTs is dependent on the characteristics of the sites present on the surface of the catalyst and on the reaction temperature. The quantity of SWNTs produced is much higher for the Ni/Al_2O_3 catalyst heat treated at 550 °C than for the Ni/Al_2O_3 catalyst heat treated at 700 °C, that presented mainly the formation of MWNTs and

amorphous carbon. However, we believe that in the near future, the production of SWNTs by decomposition of CH_4 over the catalysts developed by our group will be optimized to obtain SWNTs with high quality.

Acknowledgement

The authors acknowledge the Brazilian funding support agency: CNPq/CT-PETRO.

References

[1] F. de Bruijn, Green Chem. 7 (2005) 132–150.
[2] J.N. Armor, Catal. Lett. 101 (2005) 131–135.
[3] M.G. Poirier, C. Sapundzhiev, Int. J. Hydrogen Energy 22 (1997) 429–433.
[4] E.K. Lee, S.Y. Lee, G.Y. Han, B.K. Lee, T.J. Lee, J.H. Jun, K.J. Yoon, Carbon 42 (2004) 2641–2648.
[5] T.V. Choudhary, C. Sivadinarayana, C.C. Chusuei, A. Klinghoffer, D.W. Goodman, J. Catal. 199 (2001) 9–18.
[6] N. Muradov, F. Smith, A. T-Raissi, Catal. Today 102 (2005) 225–233.
[7] M. Inaba, K. Murata, M. Saito, I. Takahara, N. Mimura, React. Kinet. Catal. Lett. 77 (2002) 109–115.
[8] I. Suelves, M.J. Lázaro, R. Moliner, B.M. Corbella, J.M. Palacios, Int. J. Hydrogen Energy 30 (2005) 1555–1567.
[9] R. Aiello, J.E. Fiscus, H.C. zur Loye, M.D. Amiridis, Appl. Catal. A Gen. 192 (2000) 227–234.
[10] Z. Bai, H. Chen, B. Li, W. Li, J. Anal. Appl. Pyrolysis 73 (2005) 335–341.
[11] N. Shah, D. Panjala, G.P. Huffman, Energy Fuels 15 (2001) 1528–1534.
[12] N. Muradov, Catal. Commun. 2 (2001) 89–94.
[13] J. Li, G. Lu, K. Li, W. Wang, J. Mol. Catal. A Chem. 221 (2004) 105–112.
[14] Z. Bai, H. Chen, W. Li, B. Li, Int. J. Hydrogen Energy 31 (2006) 899–905.
[15] M.A. Ermakova, D.Yu. Ermakov, G.G. Kuvshinov, Appl. Catal. A Gen. 201 (2000) 61–70.
[16] Y. Li, J. Chen, Y. Qin, L. Chang, Energy Fuels 14 (2000) 1188–1194.
[17] H. Wang, R.T.K. Baker, J. Phys. Chem. B 108 (2004) 20273–20277.
[18] S. Takenaka, Y. Shigeta, E. Tanabe, K. Otsuka, J. Phys. Chem. B 108 (2004) 7656–7664.
[19] H.V. Fajardo, A.O. Martins, R.M. de Almeida, L.K. Noda, L.F.D. Probst, N.L.V. Carreño, A. Valentini, Mater. Lett. 59 (2005) 3963–3967.
[20] A. Valentini, N.L.V. Carreño, L.F.D. Probst, E.R. Leite, E. Longo, Microporous Mesoporous Mater. 68 (2004) 151–157.
[21] Q. Li, H. Yan, J. Zhang, Z. Liu, Carbon 42 (2004) 829–835.
[22] M.H. Herbst, M.I.F. Macêdo, A.M. Rocco, Quim. Nova 27 (2004) 986–992.